

Effect of travelling wave on vortex-induced vibrations of submerged floating tunnel tethers

Xiaodong Wu, Fei Ge, Youshi Hong*

State Key Laboratory of Nonlinear Mechanics, Institute of Mechanics, Chinese Academy of Sciences, Beijing 100190, China

Received 19 July 2010; revised 2 August 2010; accepted 3 August 2010

Abstract

Recently on a previously unknown phenomenon in vortex-induced vibrations (VIV) of the flexible structures with large aspect ratio (length to diameter) was discovered in field experiments, which shows that traveling wave rather than standing wave dominates the response of VIV. In this paper propagation of CF and IL responses in Submerged Floating Tunnel (SFT) has been simulated by using a modified wake oscillator, in which wake diffusion and variation of tension along the axis of tether are considered. The dominance of travelling wave in VIV has been predated. Finally the effect of the dominance of traveling wave on VIV of SFT tethers under shear flows has been addressed.

© 2010 Published by Elsevier Ltd. Open access under [CC BY-NC-ND license](http://creativecommons.org/licenses/by-nc-nd/3.0/).

Keyword: vortex-induced vibrations (VIV); traveling wave; wake oscillator

1. Introduction

The design of submerged floating tunnel touches many safety issues, of which the vortex-induced vibration (VIV) of tethers is a quite important factor. The VIV of flexible risers is very common phenomenon in many fields of engineering, as summarized in the comprehensive reviews of Sarpkaya [1], Williamson and Govardhan [2], and Gabbai and Benaroya [3]. However, most of these works are focused on the VIV of short, rigid cylinders; generally their aspect ratio (length to diameter) is no more than 100. For flexible structures with large aspect ratio such as tethers, which have a series of natural frequencies, distributed vortex-induced forces may excite several natural frequencies at high order modes. In this case, their vibrating response differs from the response of short cylinders in many aspects, including formation of traveling waves [4]. Whereas since testing this kind of model needs a large facility and relatively complicated instrumentation, there have been only a very few studies of VIV of structures with large aspect ratio, hence the features of VIV of these structures have not been fully studied.

Both standing wave and traveling wave pattern of vibration responses have been realizable in field and laboratory experiments. Vandiver [4] and Alexander [5] observed traveling wave responses for cables. Vandiver [4] gave a

* Corresponding author. Tel.: 86-10-82543966; fax: 86-10-62561284.

E-mail address: hongys@imech.ac.cn

wave propagation parameter $n\zeta_n$ to predict which type of response is to be expected, where ζ_n is damping and n is the mode number, when the parameter is less than 0.2, only standing wave behaviour is to appear over the entire cylinder, when it is greater than 0.2, besides the standing wave, traveling wave also begin to emerge. Based on this criterion, flexible structures with large aspect ratio such as tethers, which often respond at high order modes, could always be in a combination mode of traveling wave and standing wave.

According to the prior knowledge [4], for flexible structures with co-occurrence of traveling wave and standing wave, a standing wave forms in the "power-in" region, where the structure takes energy from the fluid, and energy is dissipated as traveling waves from the ends of the "power-in" region, so peak strain and fatigue damage rates are expected to locate at antinodes of standing wave. However, this is not always the case when aspect ratio of the flexible cylinder is large enough. Vandiver et al. [6] conducted experiments on flexible cylinders with very large aspect ratio in the Gulf Stream in 2004 and 2006. They surprisingly observed the energy in the standing region is very weak, while energy in traveling wave regions is very strong.

The methods for predicting VIV are usually based on the laboratory data of short, rigid cylinders, so when these methods are used to predict the VIV of structures with large aspect ratio, the results could be in great disparity with experimental data. Chaplin et al. [7] conducted laboratory experiments of VIV of a long tension riser in a stepped current at the Delta Flume of Delft Hydraulics and measured the IL and CF displacements, curvatures as benchmarks for testing 11 different methods of predicting VIV. They found, compared to the measured responses, the CF displacements and curvatures computed by these predicting methods were comparably accurate, but the IL results could not be predicted accurately by any of the predicting methods. To make up this deficiency, Ge et al. [8] developed a wake oscillator model which considering the couple of IL and CF VIV. Using this model, they found the IL curvature was not smaller than CF curvature, which indicated that both IL and CF vibrations were important for fatigue damage of structures with large aspect ratio.

This paper, as the continuation of the work of Ge et al. [8], is to study the features of IL and CF VIV of flexible tether and to our knowledge, is first to predict the dominance of travelling wave of VIV of structures with large aspect ratio by using a modified wake oscillator model, in which wake diffusion and variation of tension along the axis of tether are considered. Furthermore, the effect of travelling wave on VIV of tether, especially in the case where travelling wave is dominant, is to be discussed.

2. Model description

2.1. Structure model

The tether is assumed to be a tensioned cable which undergoes uniform or shear flow (Fig. 1). The cable has two degrees of freedom, the IL and CF displacements can be modeled as

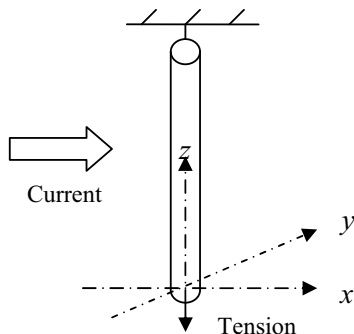


Fig. 1 Skeleton of the tensioned cable

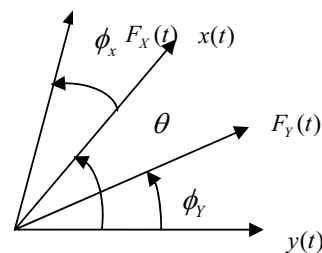


Fig. 2 Definition of phase between force and motion

$$\bar{m} \frac{\partial^2 x}{\partial t^2} + (C + C') \frac{\partial x}{\partial t} + EI \frac{\partial^4 x}{\partial z^4} - \frac{\partial}{\partial t} \left(T \frac{\partial x}{\partial z} \right) = F_x \quad (1a)$$

$$\bar{m} \frac{\partial^2 y}{\partial t^2} + (C + C') \frac{\partial y}{\partial t} + EI \frac{\partial^4 y}{\partial z^4} - \frac{\partial}{\partial t} \left(T \frac{\partial y}{\partial z} \right) = F_y \quad (1b)$$

where the mass takes into count the mass of cable and the fluid added mass per unit, reads

$$m = m_s + m_f, \quad m_f = \frac{\pi}{4} C_a \rho D^2, \quad (2)$$

C_a is the added mass coefficient, ρ is the density of water, D is the diameter of the cylinder. C is the structure damping coefficient. C' is fluid damping coefficient, parameterized as

$$C' = \gamma \Omega_f \rho D^2 \quad (3)$$

where γ is a parameter determined through experiments, while Ω_f is frequency of vortex shedding. EI is the bending stiffness, T is tension in the structure, parameterized as

$$T = T_0 + EA \frac{S - L}{L} \quad (4)$$

where A is the area of the cylinder, E is the elastic modulus, T_0 is initial tension, $S - L$ is the increase of the length, for a tensioned cable, it changes the tension and therefore the natural frequencies.

2.2. Hydrodynamic force

F in equation (1) is hydrodynamic force acting on the cable, which is in proportion to the square of current velocity, read as

$$F_x = \frac{1}{2} C_D \rho D U^2, \quad F_y = \frac{1}{2} C_L \rho D U^2 \quad (5)$$

where U is current velocity, C_D is the drag coefficient, C_L is the lift coefficient. The drag coefficient can be expressed as the sum of mean drag coefficient and fluctuating drag coefficient.

$$C_D = \bar{C}_D + \tilde{C}_D \quad (6)$$

where the mean drag includes form drag and friction drag, the mean drag coefficient equation [2] used before overestimated the mean drag, here the modified mean drag coefficient equation is adopted [9]

$$\bar{C}_D = \frac{2T}{\rho D \bar{R} U^2} \quad (7)$$

where \bar{R} are the mean radius of curvature of the structure. To model the fluctuating drag coefficient and lift coefficient, a set of non-dimensional variables q_x and q_y are introduced to satisfy the Van der pol equations

$$\frac{\partial^2 q_x}{\partial t^2} + \varepsilon_x \Omega_f (q_x^2 - 1) \frac{\partial q_x}{\partial t} + 4\Omega_f^2 q_x - \nu \frac{\partial^3 q_x}{\partial t^2 \partial z} = \frac{A_x}{D} \frac{\partial^2 x}{\partial t^2} \quad (8a)$$

$$\frac{\partial^2 q_y}{\partial t^2} + \varepsilon_y \Omega_f (q_y^2 - 1) \frac{\partial q_y}{\partial t} + 4\Omega_f^2 q_y - \nu \frac{\partial^3 q_y}{\partial t^2 \partial z} = \frac{A_y}{D} \frac{\partial^2 y}{\partial t^2} \quad (8b)$$

The time-varying drag coefficient and lift coefficient can be expressed as

$$\tilde{C}_D = C_{D0} \frac{q_x}{2}, \quad C_L = C_{L0} \frac{q_y}{2} \quad (9)$$

where the C_{D0} and C_{L0} are fluctuating drag coefficient and lift coefficient determined through experiments. ε_x , ε_y , A_x and A_y are constants estimated through experiments. ν is the wake diffusion.

When the cable begins to vibrate, the directions of fluctuating drag and lift no longer coincide with IL and CF directions, so the hydrodynamic force can be expressed as [10]

$$F_x = f_D + f_D' - f_L \dot{Y}(t) \quad (10a)$$

$$F_y = f_L + f_D' \dot{Y}(t) \quad (10b)$$

where $\dot{Y}(t)$ is non-dimensional CF velocity of cable. The displacements and forces of cable under VIV can be written as [6] (definition of phase can be seen in Fig. 2)

$$y(t) = A_y \sin(\omega t) \quad (11a)$$

$$x(t) = A_x \sin(2\omega t + \theta) \quad (11b)$$

$$f_L(t) = f_{L0} \sin(\omega t + \phi_y) \quad (12a)$$

$$f_D'(t) = f_{D0}' \sin[2\omega t + (\phi_x + \theta)] \quad (12b)$$

Substituting equations (11) and (12) into equation (10), then

$$F_y = f_L(t) + \frac{\omega A_y f_{D0}'}{2} \{ \sin[3\omega t + (\phi_x + \theta)] + \sin[\omega t + (\phi_x + \theta)] \} \quad (13)$$

According to Eq. (13), we will see that a third harmonic component appear in the lift force. Substituting Esq. (11), (12) and (13) to Eq. (10) iteratively, the lift force will include odd harmonic components and the drag force will include even harmonic components.

3. Case study

We take the Gulf Stream experiment in 2006 as our tether model. The set-up for experiment is shown in Fig. 3(a). The top end of the pipe was attached to the stern of the boat with a universal joint to provide a pinned boundary condition; a railroad wheel was attached to the bottom of the pipe to provide tension. The boat steered on various heading relative to the Gulf Stream so as to produce a sheared current, as seen in Fig. 3(b). The pipe was made of fiberglass with an HDPE liner.

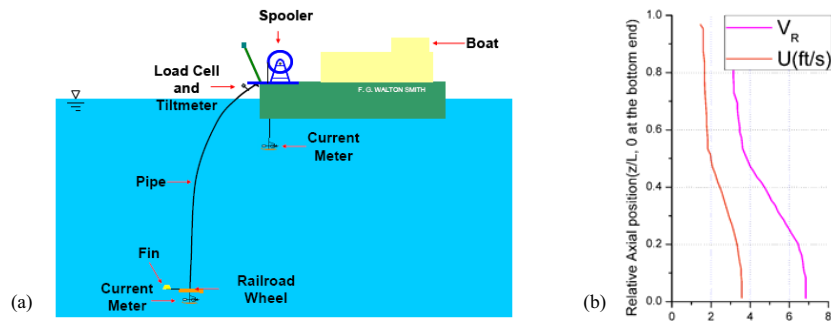


Fig. 3. (a) Set up for experiment; (b) Current speed and reduced velocity of experiment

The fluctuating drag coefficient and lift coefficient are given as 0.1 and 0.3, ν is given as 0.05. Through adjusting the model the ε_x , ε_y , A_x and A_y are selected as 0.3, 0.3, 12 and 36. The Reynolds number for this model is in range of $3.6\text{e}3$ – $3.4\text{e}4$, which is in the sub-critical range, thus Strouhal number is selected as 0.17. At initial time, the displacement and velocity of the model is 0, non-dimensional variables q_x , q_y and their first derivatives are set to 0. The pipe can be simulated as a pinned to pinned tensioned beam, so the boundary condition is set as

$$\begin{aligned} x(0,t) &= x(L,t) = 0, \dot{x}(0,t) = \dot{x}(L,t) = 0 \\ y(0,t) &= y(L,t) = 0, \dot{y}(0,t) = \dot{y}(L,t) = 0 \end{aligned} \quad (14)$$

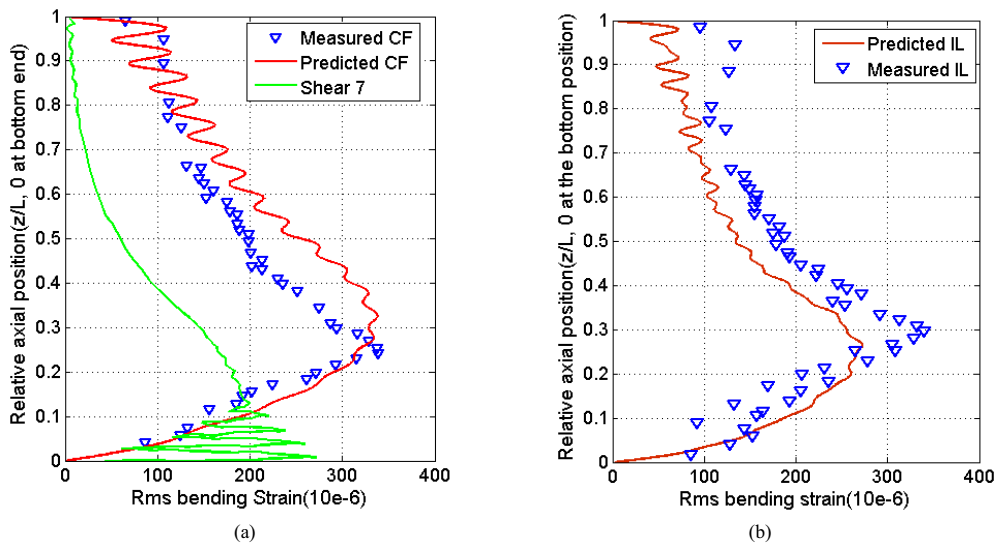


Fig. 4. (a) Rms CF bending strain; (b) Rms IL bending strain

The Rms bending strain responses in CF and IL directions are shown in Fig. 4. The effect of low frequency motion has been removed from the strain data by high-pass filtering.

As the Fig. 4 shows, the measured maximum Rms strain responses in CF and IL directions do not locate near the ends of the model, where the responses are dominated by standing waves. The measured maximum Rms strain responses are observed at about 0.3 from the bottom end. This region is dominated by traveling wave response, as seen in Fig. 5. Also seen from Fig. 4 are that the CF and IL results predicted by the modified wake oscillator

match the measured results very well, the result in CF direction given by shear7 displays serious disparity with the predicted result and shear7 code fails to predict the IL strain response. The strain responses relate to fatigue damage, the maximum Rms strain responses in CF and IL directions are nearly the same, this is consistent with recent conclusion [11,12] that the damage contributed by IL and CF VIV are of equal importance.

Fig. 5 and Fig. 6 present 90-93s strain series. A standing wave starts at the bottom boundary and persists only a very short distance. It is very less energetic. Above that region is a long traveling wave region in which the wave amplitude increases as they rise along the model. Finally the excitation region ends and the traveling wave amplitude begins to decay, at the top of the model the standing wave appears again. Its energy is also very weak. It is traveling wave region than standing wave region that holds the majority of the energy of VIV.

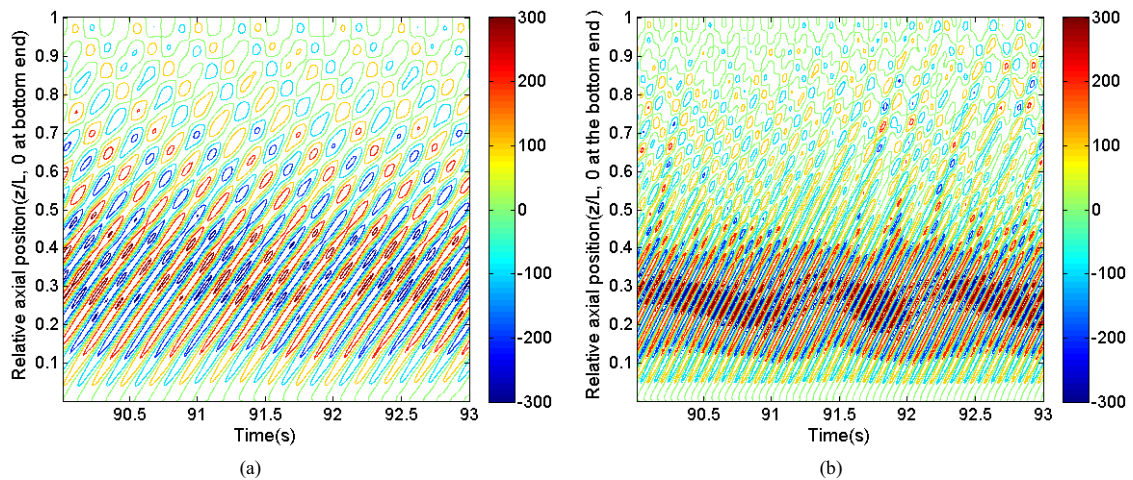


Fig. 5. (a) Predicted CF strain series; (b) Predicted IL strain series

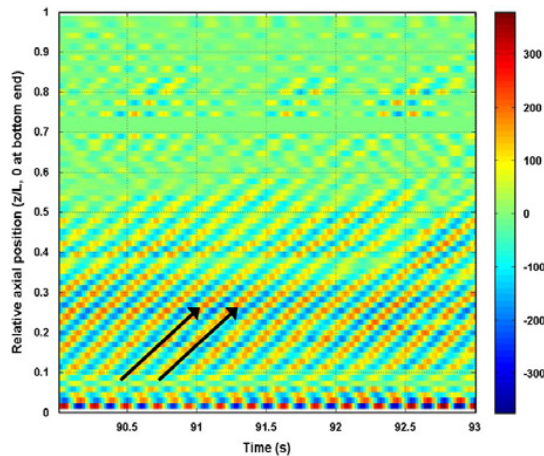


Fig. 6. Measured CF strain series [6]

According to equation (13), higher harmonic appear in lift force, this will lead to higher harmonic especially third harmonic in CF responses. If the angle between motions is in proper range, the third harmonic response will large enough. Fig. 7 shows the CF strain spectra at $z/L=0.016$ and $z/L=0.3$, where traveling wave dominates the response.

It is suggested that higher harmonic strain response is favored in traveling wave dominated region. Higher harmonic strain responses mean the large numbers of cycle and will be more likely to cause fatigue damage.

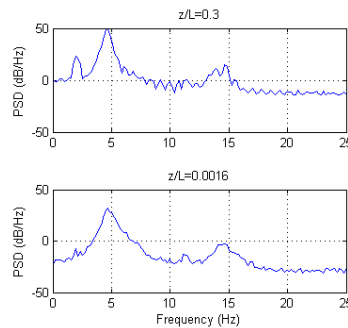


Fig. 7. CF strain spectra at two positions

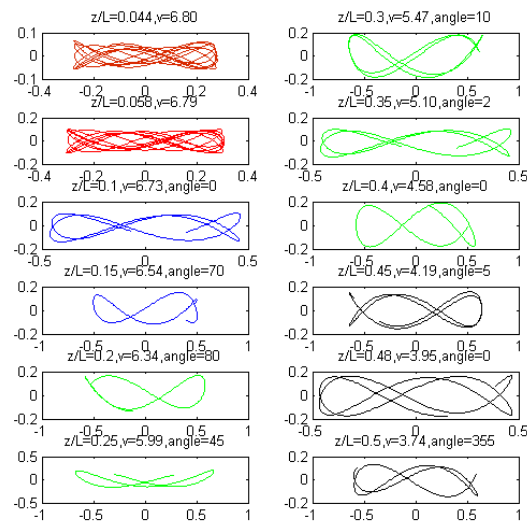


Fig. 8. Predicted motion trajectories from $z/L=0.044$ to $z/L=0.5$

Another method that confirms the higher harmonics is motion trajectory, as shown in Fig. 8. Dahl [13] shown the phase angles between 315 degree and 90 degree are favorable for large amplitude VIV, leading to large third harmonic lift forces, phase angles out of this range are unfavorable for VIV. Fig. 8 is composed of four distinct color coded regions. The motion trajectory, as well as reduced velocity, z/L location and angle between motions at some z/L locations are given. The first region is standing wave region, where phase angles are unstable, thus alternating favorable and unfavorable regions are included in this region. The second region is from $z/L=0.10$ to 0.2 , where angles between motions are stable and change very little along z/L location, this region consists favorable regions and the amplitude of strain response begin to increase. The third region comes from $z/L=0.2$ to 0.4 , where angles between motions are stable and change greatly along z/L location, and yet this region is traveling wave dominated region. The angles in this region are favorable for VIV. The amplitude of strain response continues to increase and reaches maximum in this region. The fourth region goes from $z/L=0.4$ to 0.5 , where angles between motions are stable and change very little along z/L location, this region also consists favorable regions. However since the wave decay is very considerable, the strain response begins to decrease. For flexible structure with large aspect ratio,

phase angles in traveling wave dominated region are propitious for higher harmonic forces and therefore higher harmonic response.

4. Conclusions

The propagation of CF and IL responses in VIV of flexible tether with large aspect ratio has been simulated with a modified wake oscillator model. The result shows that for flexible tether with large aspect ratio, traveling wave other than standing wave dominates the response, and when travelling wave dominates the response, the maximum Rms strain response is observed in regions dominated by traveling wave response and not near the ends of the model. Compared to standing wave regions, the regions dominated by traveling wave response are more favorable for higher harmonic, which more likely cause fatigue damage.

It should be noticed that the Eq. (7) can be used to combine the higher harmonic to wake oscillator model qualitatively, however, the predicted third harmonic responses are relatively small. The VIV of flexible cylinder with large aspect ratio are along with the emergence of multi-vortex, which multiplies the third harmonic lift force, so the higher harmonic force model in Eq. (7) should be corrected in this case.

Acknowledgments

This paper is supported by National Natural Science Foundation of China (nos. 10532070, 10772178) and Knowledge Innovation Program of Chinese Academy of Sciences (no. KJCX2-YW-L07).

References

- [1] Sarpkaya T. A critical review of the intrinsic nature of vortex-induced vibrations. *Journal of Fluids and Structures* 2004; 19(4): 389-447.
- [2] Williamson CHK, Govardhan R. Vortex-induced vibrations. *Annual Review of Fluid Mechanics* 2004; 36: 413-455.
- [3] Gabbai RD, Benaroya H. An overview of modeling and experiments of vortex-induced vibration of circular cylinders. *Journal of Sound and Vibration* 2005; 282(3-5): 575-616.
- [4] Vandiver JK. Dimensionless parameters important to the prediction of vortex-induced vibration of long, flexible cylinders in ocean currents. *Journal of Fluids and Structures* 1993; 7(5): 423-455.
- [5] Alexander CM. The complex vibrations and implied drag of a long oceanographic wire in cross-flow. *Ocean Engineering* 1983; 8(4): 379-406.
- [6] Vandiver JK, Jaiswal V, et al. Insights on vortex-induced, traveling waves on long risers. *Journal of Fluids and Structures* 2009; 25(4): 641-653.
- [7] Chaplin JR, Bearman PW, et al. Blind predictions of laboratory measurements of vortex-induced vibrations of a tension riser. *Journal of Fluids and Structures* 2005; 21(1): 25-40.
- [8] Ge F, Long X, et al. Flow-induced vibrations of long circular cylinders modeled by coupled nonlinear oscillators. *Science in China, Series G: Physics, Mechanics and Astronomy* 2009; 52(7): 1086-1093.
- [9] Jhingran V, Jaiswal V, et al. Spatial variation of drag on long cylinders in sheared flow. New York, Amer Soc Mechanical Engineers.
- [10] Wang XQ, So RMC, et al. A non-linear fluid force model for vortex-induced vibration of an elastic cylinder. *Journal of Sound and Vibration* 2003; 260(2): 287-305.
- [11] Trim AD, Braaten H, et al. Experimental investigation of vortex-induced vibration of long marine risers. *Journal of Fluids and Structures* 2005; 21(3): 335-361.
- [12] Baarholm GS, Larsen, CM, et al. On fatigue damage accumulation from in-line and cross-flow vortex-induced vibrations on risers. *Journal of Fluids and Structures* 2006; 22(1): 109-127.
- [13] Dahl JM, Hover FS, et al. Resonant vibrations of bluff bodies cause multivortex shedding and high frequency forces. *Physical Review Letters* 2003; 99(14).